Grasp Prediction Toward Naturalistic Exoskeleton Glove Control

Raghuraj Chauhan, Bijo Sebastian, *Student Member, IEEE*, and Pinhas Ben-Tzvi, *Senior Member, IEEE*

***Abstract*—This paper presents accurate grasp prediction algorithms that can be used for naturalistic, synergistic control of exoskeleton gloves with minimal user input. Recent research in exoskeleton systems has focused mainly on the development of novel soft or hard mechanical designs and actuation systems for rehabilitative and assistive applications. On the other hand, estimating user intent for intelligent grasp assistance is a problem that has remained largely unaddressed. As demonstrated by existing studies, the complex motions of human hand can be mapped to a latent space, thereby reducing perceived noise in individual joint angles as well as the number of variables upon which the prediction must be performed. To this extent, we present two latent space grasp prediction algorithms for intelligent exoskeleton glove control. The first presented algorithm is based on a linear regression to determine the slope and prediction horizon. The second algorithm is based on a Gaussian process trajectory matching where the trajectory of the grasping motion is probabilistically compared to existing data in order to form a prediction. Both algorithms were tested on published motion data collected from healthy subjects. In addition, the experimental validation of the algorithms was done using the RML glove (Robotics and Mechatronics Lab), which yielded similar prediction accuracy as compared to the simulation results. The proposed prediction algorithm can act as the backbone for a shifting authority controller that simultaneously amplifies the user's motion while guiding them toward their desired grasp. Preliminary work in this direction is also described in the paper, with directions for future research.**

***Index Terms*—Exoskeleton, grasping, haptics, man-machine system, orthosis, upper limb.**

I. Introduction

INJURIES that limit or terminate one's use of their hands lead to drastic reductions in quality of life. Such injuries prevent successful interaction with and manipulation of everyday objects, such as a bag of groceries, a pencil, or even a cup of coffee [1]. Among other factors, a stroke [2] or brachial plexus injury [3] can result in such an impairment. Separate from diagnosed conditions, 1.23 million American adults have difficulty grasping or handling small objects as per the most recent U.S. census (2014) [4]. In this regard, exoskeleton gloves have emerged as an effective solution toward providing rehabilitation and/or assistance for individuals suffering from hand disabilities [5].

Over the past few decades, exoskeleton gloves have seen increased interest, especially for uses in virtual reality, as assistive devices in industrial and military applications, and for medical rehabilitation. Many novel designs have been presented, showcasing a variety of actuation methods including rigid linkages and soft coupling systems such as those in [6]–[8]. Hard linkage based designs can ensure precise joint angles and force transmission while ensuring repeatably of the grasp trajectories. On the other hand, soft systems are usually more form fitting and can ensure safety and comfort for the users hand by virtue of the materials used in the glove. More recently, there have been efforts to couple the form fitting and comfortable nature of the soft glove design with the rigid linkage based systems to guide the finger motion resulting in hybrid designs that combine the advantages of both these design paradigms [9].

Despite the major advancements in terms of exoskeleton glove design, little exploration has been made into the user guided control of these gloves. A review of exoskeleton gloves and their control methods shows a prevalence of both finger joint position sensors as well as electromyography (EMG) sensors [10] to determine user intent. However, the signals from EMG sensors are often inconsistent and require extensive training for effective operation [10]–[12]. As of now, EMG sensing technologies are not mature enough to distinguish between various kinds of grasps at an acceptably high success rate. Other approaches that explored the use of muscles on other body parts to generate the EMG signals require sensing elements to be placed at those points which, beyond being unintuitive, can induce discomfort when used for prolonged periods of time. Performing fully autonomous grasps for the wide variety of activities of daily living (ADLs) by relying only on perception of the surroundings (such as through a vision system) is in development [13], but this requires additional equipment, making the overall setup cumbersome. Similar issues arise when attempting to track the human eye to estimate grasp intentions of the user, as performed by Noronha *et al.* in [14].

A complicated orthosis, such as the hand exoskeleton with multiple degrees of freedom (DOF), requires a high level of intelligence in order to realize the plethora of actions that humans take while dealing with objects and situations encountered in daily life. This in turn points toward the need for grasp prediction

Manuscript received March 6, 2019; revised June 17, 2019; accepted August 10, 2019. Date of publication September 19, 2019; date of current version January 14, 2020. This work was supported in part by the Eunice Kennedy Shriver National Institute of Child Health and Human Development of the National Institutes of Health under Award Number R21HD095027. The content is solely the responsibility of the authors and does not necessarily represent the official views of the National Institutes of Health. This article was recommended by Associate Editor J. Wachs. *(Corresponding author: Pinhas Ben-Tzvi.)*

The authors are with the Robotics and Mechatronics Lab, Mechanical Engineering Department, Virginia Polytechnic Institute and State University, Blacksburg, VA 24060 USA (e-mail: raghur1@vt.edu; bijo7@vt.edu; bentzvi@vt.edu).

Color versions of one or more of the figures in this article are available online at http://ieeexplore.ieee.org.

Digital Object Identifier 10.1109/THMS.2019.2938139

algorithms that can leverage human inputs to provide accurate predictions.

In this regard, the focus of this paper is to provide a grasp prediction algorithm that monitors the motion of the user to come up with accurate predictions. The proposed prediction algorithm could form the backbone of controllers that aim to provide assistance to users in performing ADLs. When compared to existing state-of-the-art systems, the above approach would emphasize naturalistic motion and seamless human-exoskeleton interaction based on a novel set of grasp prediction algorithms.

Before going into the details of the proposed grasp prediction algorithms, a brief overview of the anatomy of the hand and some insight to the various grasps is provided below. The human hand, despite its complexity, has been well characterized in terms of its layout and common configurations. The kinematic model of the human hand can be constructed such that there are 21 DOF [15]. Four are allocated to each finger: the metacarpophalangeal (MCP), proximal interphalangeal (PIP), and distal interphalangeal (DIP) joints, along with adduction and abduction of the finger. The remaining five are for the thumb: the MCP and trapeziometacarpal joints have two each for flexion and adduction as well as a single DOF for the interphalangeal joints. Other sources employ models with 26 possible DOFs [16]; however, this paper is concerned with only the motion of the finger joints and will adopt the 21 DOF model that will later be reduced to only 12 independently actuated DOFs.

Common grasping configurations of the human hand, heretofore simply called *grasps*, have been studied and categorized based on ubiquity and utility in situations as specific as machining [17] or as general as those used in the common household [18]. These common grasps have been taxonomically grouped to reduce the sheer number of possibilities and unique actions humans take. A summary and subsequent marriage of previously developed taxonomies is presented by Feix *et al.* in [19]. The GRASP taxonomy therein contains only the 33 grasps that are the basis for modern studies, including the HUST dataset that is used in this paper [20]. The HUST dataset contains motion data from 30 healthy male and female subjects performing each of the 33 grasps.

Trends can be observed in existing literature regarding the effective number of DOFs in the hand. First described by Santello *et al.* in [21], a principal components analysis (PCA) on the joint angles exhibited during grasps quantitatively shows that there are effectively six DOFs to generate the overall posture of the hand. Other DOF exist in this framework that contribute to the smaller movements of the hand responsible for complex or fine tasks. Prior work in [22] demonstrates a clear clustering of grasps in the latent space which precipitates the hypothesis that PCA can be used to transform finger joint data as a first step to facilitate early prediction of grasp intention. The use of reduced number of PCs allow for the complexity of hand motion to be greatly simplified from a modeling perspective by reducing the requisite number of DOFs to sufficiently represent each grasp. Furthermore, a PCA is known to be able to reduce the magnitude of noise in data [23] and is therefore a useful tool in the mitigation of the unintentional, minute movements an impaired individual can make while executing a grasp. Based on these factors, we used only the first six PCs for this paper.

This paper presents two grasp prediction algorithms, one based on regression of motion data and another that uses the probabilistic comparison of executed trajectories to accurately predict an intended grasp within a short duration (approx. 25% of the grasp) from the start of motion. Simulation and formulation of these algorithms was completed using the HUST dataset and validation was performed using the RML Glove whose fundamental mechanics are presented in [9]. These tests serve a secondary purpose, allowing us to characterize the relationship between unconstrained motion (HUST) and constrained motion (RML Glove), as well as the effects of constrained motion on the clustering and predictability of human grasping. These prediction schemes can be used in a haptic controller to assist the user of an exoskeleton glove when they are unable to successfully maneuver their hands of their own volition. Section II of this paper will present our existing regression-based prediction algorithm [24] and our new probabilistic comparison algorithm while highlighting the improvements in performance shown by the newer approach. Section III will discuss the experiments conducted using the RML Glove and the results of both the simulations and the experiment. Section IV will present a controller that makes use of the prediction algorithm to guide the user's motion while wearing the glove. Finally, Section V will conclude this paper.

II. Prediction Algorithms

A. PCA and Dimensional Reduction

While a brief formulation is provided in the following section for the use of PCA, the reader is referred to [21], which contains a more detailed discussion of the process and the variations between individuals. This section will focus on the specific formulation based on the HUST dataset. As previously mentioned, the data were collected from 30 healthy individuals, equally male and female, who were instructed to grasp different objects, with three trials for each object. There were three objects for each of the 33 grasps resulting in 297 trials per subject. The data for each trial contain joint angle information from the start of motion to the completion of the grasp at regular intervals. This dataset does not include information about the adduction of digits reducing the number of DOFs from 21 to 16. It is known that for the four fingers, the DIP joint is highly coupled to the PIP joint during contact free motion of the hand [25]. Therefore, by observing these relationships, the hand can be considered as only a 12-DOF system. As previously stated, the pose of the human hand defined by these DOFs is given by

$$\vec{\theta} = [\theta_1, \theta_2, \ldots, \theta_{12}] \tag{1}$$

where $\theta_{i=1-12}$ is the ith joint of the hand. The final pose vector of each trial $\vec{\theta}_{i=1-297}$ per subject is combined in the design matrix, $\mathbf{X} \in \mathbb{R}^{297\times 12}$, as given by

$$\mathbf{X} = \left[\vec{\theta}_1, \vec{\theta}_2, \ldots, \vec{\theta}_{297}\right]^T \tag{2}$$

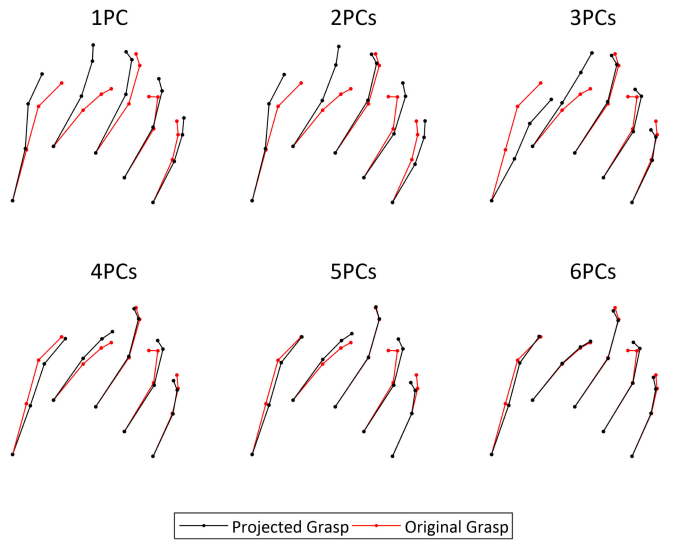

Fig. 1. Reconstruction of Grasp 17, index finger extension, using an increasing number of principle components. The six images shown are each of an entire hand (five fingers) in the final configuration of Grasp 17.

where the data in $\mathbf{X}$ have been mean centered. Determination of the normalized eigenvalues λ_i and corresponding eigenvectors (principal components) $\mathbf{W}$ of the covariance of the design matrix $\mathbf{X}^T\mathbf{X}$ results in PCs that are used to map the original poses, $\vec{\theta}$ into a lower dimensional space, $\vec{\phi}$, via (4)

$$\mathbf{W} = \left[\vec{PC}_1, \vec{PC}_2, \ldots, \vec{PC}_p\right] \tag{3}$$

$$\vec{\phi} = \vec{\theta}\mathbf{W}. \tag{4}$$

The terms in $\mathbf{W}$ are ordered such that $\vec{PC}_1 \in \mathbb{R}^{12\times 1}$ has the largest corresponding eigenvalue λ_1 and since only six PCs are to be considered, $p = 6$. PCs with larger respective eigenvalues or weights capture a greater variance of the data in $\mathbf{X}$ and are therefore more significant. It is to be noted that the column vectors in $\mathbf{W}$ are the configuration of each PC in the original joint space. The effects of using an increasing number of PCs are shown in Fig. 1 where a greater number of PCs are used to generate a more accurate reconstruction. It should be noted that most of the figures in this paper are best viewed in color.

B. Regression-Based Prediction

Measured finger joint data are mapped into the lower dimensional space and regressed using

$$\vec{\psi}(t) = \vec{\phi}(t) + \vec{\beta}(t)\tau_t^+ \tag{5}$$

where $\vec{\psi}$ and $\vec{\beta}$ are, respectively, the extrapolated poses and regression slopes at the current time t for each PC, and τ_t^+ is the predicted grasp completion time. The regression for each PC is calculated for the following iteration using amounts of data $\tau_{i,t+1}^-$ given by

$$\tau_{i,t+1}^- = \tau_0^-(1 + |1 - \zeta\beta_i(t)|) \tag{6}$$

where τ_0^- and ζ are tunable parameters that are constant for all PCs and i refers to each PC. The values for the tunable parameters in (6) was chosen empirically, such that less prior data are used for a more quickly moving PCs.

The predicted grasp completion time for the next iteration τ_{t+1}^+, mutual to all the considered PCs, is calculated to minimize the error between each regression line, defined by β_i, and the g possible final configurations for the search set of known grasps

$$\tau_{t+1}^+ = \frac{1}{g}\sum_{j=1}^{g} \underset{\tau_{t+1}^+}{\operatorname{argmin}} \left[\sum_{i=1}^{p} \frac{|\beta_i(t)\tau_{t+1}^+ - \phi_j + b_{i,j}|}{p\sqrt{\beta_i(t)^2 + 1}}\right]. \tag{7}$$

The outer summation includes all the grasps in the search set, and the inner summation includes all the considered PCs. The initial pose for each grasp in the search set is $b_{i,j}$. The grasp set can be reduced to contain only seminal grasps ($g = 8$) in the categorization presented in Section III, thereby reducing the computational load.

Selection of the most likely grasp after the regression is accomplished using

$$s_k(t) = \sum_{i=1}^{p} \lambda_i \left|\frac{(\phi_{i,k} - \psi_i(t))^\gamma}{\phi_{i,k}}\right| \tag{8}$$

$$c_k(t) = \int_0^t \alpha(1 - s_k(t) - \mu)^\sigma dt \tag{9}$$

where $s_k(t)$ and $c_k(t)$ are the momentary score and confidence for each of the possible grasps. In (8), the score is calculated as a weighted average of the percentage errors between each of the extrapolated PC magnitudes and each of the known PC magnitudes, weighted by their respective eigenvalues. The confidence in (9) is the integral of the excess between the score and μ. The μ term is used to penalize the confidence $c_k(t)$ when $s_k(t) < \mu$. The terms γ, α, and σ are additional tuning parameters. Once the confidence exceeds a predefined threshold, such that $c_k(t) \geq c_{k_{\min}}$, the corresponding grasp becomes the predicted grasp. The effects of changing this threshold are discussed in Section III.

C. Trajectory-Based Prediction

1) Gaussian Process Modeling: The trajectory-based prediction algorithm formulates each set of measured grasp data as a Gaussian process with which the trial data can be probabilistically compared. A more detailed description of the Gaussian process formulation can be found in [26].

The measurement data for each trial, dimensionally reduced to the principal components, is time scaled to range from zero to one and then resampled at m points to maintain uniformity. It can be considered that the time t corresponding to each measurement $\vec{\phi}$ is the progress along the p-dimensional curve taken to perform each grasp. The nine trials for each grasp are then aggregated so that each of the m measurements can be considered as a Gaussian distribution $\mathcal{N}(\mu_{\phi_{i,j}}, \sigma^2_{\phi_{i,j}})$, where i refers to the DOF and j refers to position along the curve (t).

From this data, the Gaussian process for each dimension for each grasp is formulated with the radial basis function as

the kernel

$$p(t,t') = \sigma_f^2 \exp\left[\frac{-(t-t')^2}{2l^2}\right] + \sigma_{\phi_i}^2 \delta(t,t') \tag{10}$$

where σ_f^2 and l are the allowable process covariance and length factor hyperparameters, and δ is the Kronecher delta. The term $\sigma_{\phi_i}^2$ is variance in the trial data at the time t. Since its value is only considered when $t = t'$ due to the Kronecher delta, it can be assumed that $\sigma_{\phi_i}^2 = \sigma_{\phi_{i,j=t}}^2$. The values for the hyperparameters were tuned to yield smooth curves that did not overfit the priors. The resulting covariance matrix K is used from a regression at m' points along $\vec{t}_s$, also ranging from zero to one, using

$$K_* = [p(t_*,t_1), p(t_*,t_2), \ldots, p(t_*,t_m)] \tag{11}$$

$$K_{**} = p(t_*,t_*) \tag{12}$$

$$\Phi_{i,j} = \mathcal{N}(K_* K^{-1} \vec{\mu}_{\phi_i},\ K_{**} - K_* K^{-1} K_*^T) \tag{13}$$

where t_* is the time, in $\vec{t}_s$, of the point being regressed and $\mathbf{\Phi} \in \mathbb{R}^{p \times m_g}$ is the matrix of random variables corresponding to the p DOFs and m_g instances, and has expected values and variances of $\vec{\mu}_{\Phi_{i,j}}$ and $\vec{\sigma}^2_{\Phi_{i,j}}$ at each index. The vector $\vec{\mu}_{\phi_i} \in \mathbb{R}^m$ refers the original expected values of the ith DOF. The resulting process is shown in Fig. 2 for a single grasp. The above process is completed for each grasp once offline.

2) Trajectory Matching: Measured data points, mapped to the latent variable space, are compared to each of the processes for each of the grasps. The joint log-likelihood of the measurements ($\phi_{i,j}$) belonging to each process ($\Phi_{i,j}$) is calculated to determine a measure of similarity

$$L_k(\vec{t}) = \sum_{i=1}^{p} \sum_{j=1}^{n} \ln\{\mathcal{L}[\phi_{i,j} \mid (\mu_{\Phi_{i,j'}},\ \sigma^2_{\Phi_{i,j'}})]\} \tag{14}$$

where n is the number of data points available. To expedite this calculation, the values pertaining to $\Phi_{i,j'}$ are not drawn from the process at the time of measurement t_m as re-evaluation of (11)–(13) requires unnecessary computation. Rather, the value is drawn from $\vec{\Phi}_i$ at an index j', where

$$j' = \underset{j}{\operatorname{argmin}} |j' - \vec{t}_s| \tag{15}$$

resulting in a look-up table implementation of the Gaussian process.

Furthermore, the original formulation of the Gaussian processes involved the time scaling that sets all the grasps times equal. This is certainly not representative of natural human action as various tasks take different amounts of time, to say nothing of the effects due to the physical impairment of the users. Therefore, the measurement data must be adaptively scaled to fit each grasp for comparison using

$$\rho_k = \underset{\rho_k}{\operatorname{argmax}}(L_k(\vec{t}_k)), \vec{t}_k = \rho_k \vec{t}_m \tag{16}$$

where ρ_k is the scaling factor for the measurement times for each possible grasp. This can be considered as evaluating the likelihood of the measurement at the closest point on the curve. Equivalently, the l_2-norm could be evaluated as the objective

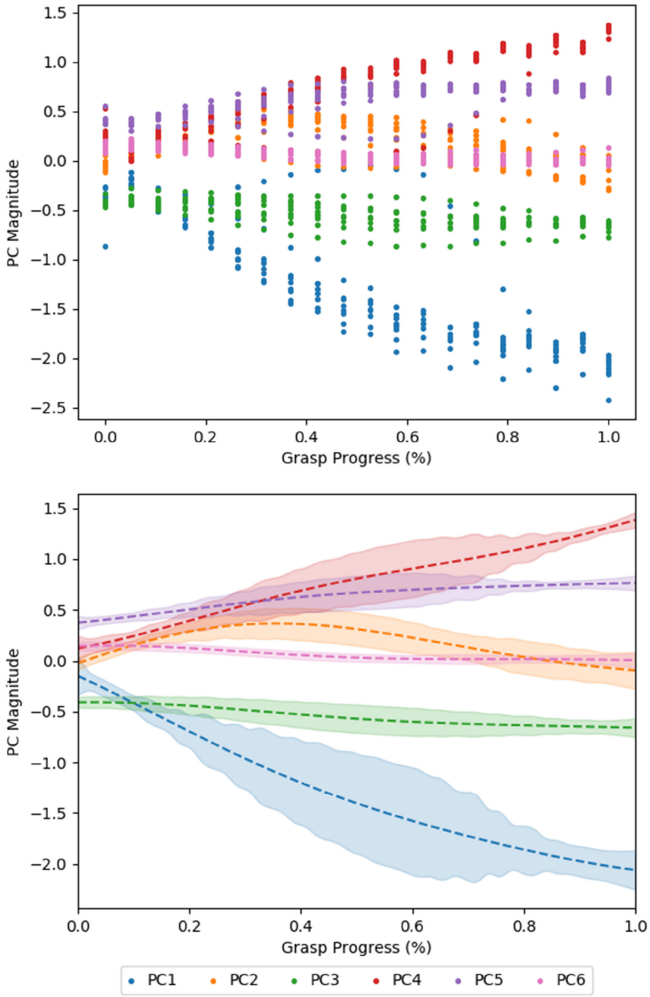

Fig. 2. Comparison of the original, time scaled, resampled motion (top) and the Gaussian process (bottom) for Grasp 21 tripod variation. The dashed lines and shaded regions in the bottom plot are the process expected values, $\mu_{\Phi_{i,j}}$, and standard deviation, $\sigma^2_{\Phi_{i,j}}$, respectively.

function instead of the likelihood for simplicity. The most likely grasp is then, simply, the one for which $L_k(\vec{t}_k)$ is greatest or

$$k_{\text{pred}} = \underset{k}{\operatorname{argmax}}(L_k(\vec{t}_k)) \tag{17}$$

where k_{pred} is the predicted grasp. It is required that the likelihood is evaluated here, not the l_2-norm.

To account for motion that can have frequent starts and stops, the scaling factor can instead be treated as a vector $\vec{\rho_k} \in \mathbb{R}^{1 \times n}$. This formulation allows for not only nonuniform time scaling but also for maintaining a fixed pose for a period of time. In this case, to prevent artificially increasing the results of (14), only points that satisfy

$$||t_{k,j}, t_{k,j+1}||_2 \geq r \tag{18}$$

for an r of some small value. Therefore, adjacent indexes of $\vec{t}_k$ at j and $j+1$ must have a distance of at least r along the trajectory. It should be noted that $\vec{t}_{k,s}$ can be allowed to be semimonotonically increasing due to the unsteady motion of an impaired hand; however, while not present in the HUST dataset

Algorithm 1: Grasp Prediction Algorithm, argmax($\vec{L}'$).

for each grasp, k **do**
  $\vec{t}_m = t_0$
  while $t_{k,0} - 0 \geq \epsilon$ **do**
    $l_k = \text{length}(\vec{t}_m)$
    for each time in $\vec{t}_m$, j **do**
      calculate $\rho_{k,j}$, $t_{k,j}$
    end for
    $\vec{t}_m \leftarrow [t_{-l_m}, \vec{t}_m]$
  end while
  calculate L'_k and argmax($\vec{L}'$)
end for

TABLE I
PERFORMANCE RESULTS FOR ALL SUBJECTS USING BOTH PREDICTION ALGORITHMS

	Heuristic Acc.		Absolute Acc.		% Motion Required	
	Mean	*Std. Dev.*	*Mean*	*Std. Dev.*	*Mean*	*Std. Dev.*
Reg.	78.76	10.79	29.29	7.23	26.29	4.21
Traj.	76.45	6.13	71.38	6.33	*	*

TABLE II
GRASP GROUPINGS

Group	Grasp Number(s)
Cylindrical Wrap	1, 2, 3
Sphere	11, 13, 14, 26, 27, 28
Two Finger Pinch	9, 24, 31, 33
Prismatic Small Stick	6, 7, 8, 20, 25, 21, 23
Index Extension Wrap	17, 19, 29, 32
Disk	10, 12
Flat Parallel	18, 22
Adducted Thumb Wrap	4, 5, 15, 16, 30

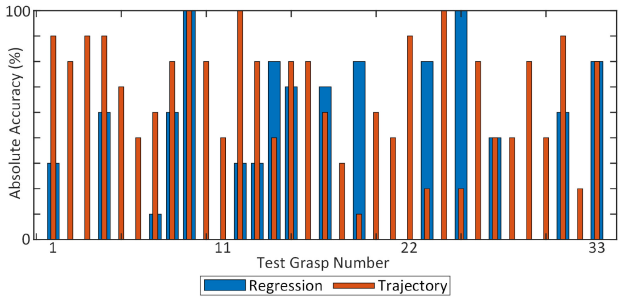

Fig. 3. Absolute prediction accuracy for all 33 grasps by subject 1. The accuracy of the trajectory-based prediction (orange) is, in general, higher than that of the regression-based prediction (blue).

or a normal part of human grasping, the hand motion could be returning to its starting configuration without completing the grasp which would be indicated by a continued negative monotonicity at the end of $\vec{t}_{k,s}$. The issue here is to determine when the motion has started and what window of the user's motion needs to be used in the grasp selection. A solution would be to determine $\vec{\rho_k}$ in a reverse order, starting with the most recent measurement, and closing the window once the start of the grasp has been met within some tolerance ϵ. Since this process allows for a different number of points to be used for each grasp, the value for $L_k(\vec{t}_k)$ must be normalized by the length of $\vec{t}_k$ via

$$L'_k = L_k(\vec{t}_k)/l_k \tag{19}$$

where l_k is the number of indices in $\vec{t}_k$, and L'_k is the normalized value. The step for this prediction is shown in Algorithm 1.

III. EXPERIMENTAL VALIDATION

A. Simulation

Experimental simulation results for the prediction algorithms presented in the previous section were completed using individual trials from the HUST dataset. For both sets of experiments, each joint angle data point was augmented with random noise as given below

$$\theta_e = \theta + \mathcal{U}(-5^\circ, 5^\circ) \tag{20}$$

where θ_e is the noisy value used in the prediction algorithm. In the case of the second algorithm, the time indexes of the data were expanded by a factor of 1.5 to necessitate the use of (15). Additionally, in the formulation of the covariance matrices for each subject, the trial data were excluded to prevent overfitting to the model. The results of the algorithms are shown in Table I. The trajectory-based prediction does not require a condition to be met for a grasp prediction to occur; therefore, for uniformity, the accuracy values presented are for when the trial is 25% complete. One metric used is the absolute accuracy where the prediction grasp number and tested grasp number are the same. Alternatively, heuristic accuracy in the prediction is established if absolute accuracy or either of the following criteria is achieved.

1) The predicted grasp and the test grasp occupy the same group according to Table II. The groups were determined based on similar object interaction.
2) The mean joint angle error between the predicted and test grasp does not exceed 20°, which indicates a geometric similarity that accounts for permutations in grasps unique to individuals.

These criteria exist only as a metric for the performance of the grasps.

The absolute accuracy for each grasp for subject 1 using both prediction algorithms is shown in Fig. 3. While both have similar heuristic accuracies according to the listed performance metrics, it is clear to see that the trajectory-based prediction has a much higher absolute accuracy: 29.29% versus 71.38%, as given in Table I. The specific prediction results for both prediction algorithms is shown in the confusion matrices in Fig. 4. A high absolute accuracy is indicated by a high number of occurrences (dark blue) along the main diagonal of each plot. The accuracy of the regression-based prediction is a result of using tuning parameters α, σ, μ, and γ, which maximize the performance for all subjects.

1) Regression-Based Prediction Results: By choosing more appropriate tuning parameters for each individual, higher grasp prediction fidelity can be achieved. In the case of subject 1, an accuracy of 90% was achievable, by manually tuning the parameters. The remainder of the discussion into this algorithm's performance shall, for simplicity, continue to focus on subject 1;

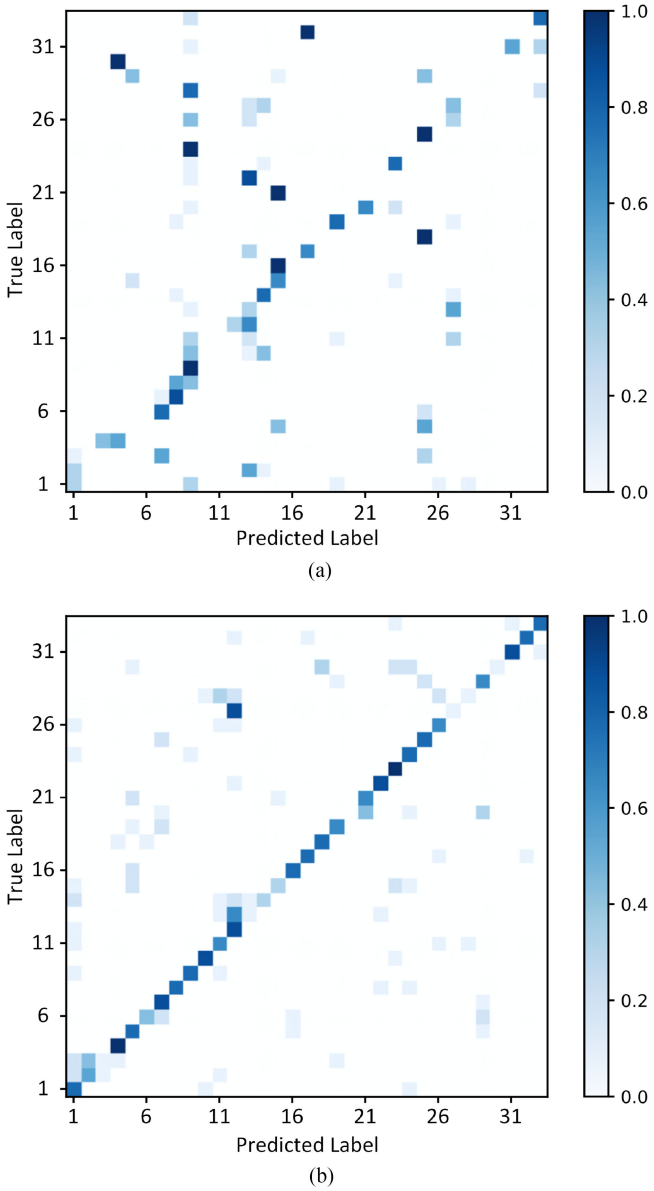

Fig. 4. Confusion matrices that result from the regression-based prediction (a) and the trajectory-based prediction (b) for subject 1 after 25% of the motion has completed. The number of occurrences for each prediction is colored according to the bars on the right. The prediction for the regression-based algorithm was tested using parameters that maximize the results for all subject.

however, the results shown can be achieved by any of the subjects.

In several cases, the errors in grasp prediction are minimal. For example, when testing the worst performing grasp, Grasp 2, the incorrect predictions of Grasp 13 and Grasp 14 had average joint angle errors of 22.11° and 25.68°, respectively. Both errors are small enough to reinforce the fact that the algorithm still produces grasps close to the intended one and therefore, can be used in the proposed control scheme as described later in this paper.

Converging to another grasp within the same group from Table II is acceptable because the groups contain grasps that only interact with objects in a similar fashion. This requirement means that these grasps, by necessity, have a similar configuration. Fig. 5 shows the configuration for the grasps in the two finger pinch group. Grasps in this group interact with an object using the thumb and the index finger. The remaining digits do not interact with the object and, therefore, remain out of the way. It can be seen that specific configuration of those remaining digits are nebulous since they do not perform any specific function. For an individual with an impairment trying to manipulate an object using only their thumb and index finger, any of these grasps would suffice.

The effects on the accuracy and speed of varying the threshold parameter μ can be seen in [24] where a larger threshold required an increased percentage of the grasp to be completed before (9) converges. Similar effects are seen for varying α, σ, and γ. This is due to the grasp decision still being made on the error between each PC configuration, $\phi_{i,k} - \psi_i(t)$.

2) Trajectory-Based Prediction Results: The trajectory-based prediction displays objectively higher fidelity to the test/desired grasp. As shown in Fig. 3, the trajectory-based prediction determines the actual test grasp with much higher frequency. For many grasps, it can be seen that the regression-based prediction never predicts the correct grasp. As discussed in [24], while it is acceptable to converge to a similar grasp, continued iterations of the prediction as more of the grasp is completed is likely to converge to the absolute intended grasp. The trajectory-based prediction is superior in this regard, as only a single run of the prediction, lasting less than one quarter of the grasp motion, results in this absolute determination.

The stochastic treatment of each grasp allows for more instantaneous grasp predictions as a likelihood evaluation using (14) and (16) can be performed with a single measurement. Fig. 6 shows the heuristic and absolute accuracies in the prediction for all subjects. There is a clear trend that, as the amount of the motion completed increases, so does the chance of the prediction being accurate by up to approximately 20%.

In Fig. 7, the L'_k values for each of the grasps during a trial of Grasp 14 tripod are displayed. At the start of trial, Grasp 27 quadpod appears to be the most likely grasp. These two grasps are used to hold a small object of approximately the same size with three or four fingers, respectively. It follows that both motions would initially be likely candidates in this case. In Fig. 7(b), the trend can be more clearly seen that unlikely grasps have a decreasing L'_k over time.

B. Hardware Experiment and Results

The two prediction algorithms were conducted on data collected using the a glove prototype based on the mechanism in [9].

1) Experimental Setup: The RML Glove is a lightweight exoskeleton designed to unobtrusively guide the user's hand in naturalistic motion profiles. This exoskeleton glove mechanically couples the motion of each finger joint so that they move in a trajectory that best approximates the natural closing and opening motion of a hand. This is accomplished via a dual four-bar mechanism shown in Fig. 8 and described in greater detail in [9]. The original design of the glove in that work

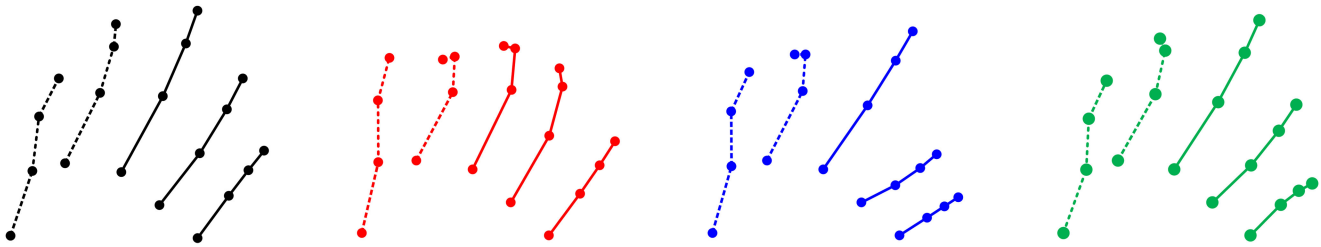

Fig. 5. Reconstructed configurations of the grasps within the two finger pinch group from Table II as demonstrated by subject 1 are shown in the figure, from left to right: Grasp 9 palmar pinch (black), Grasp 24 tip pinch (red), Grasp 31 ring (blue), Grasp 33 inferior pincer. Grasps in this group exhibit similar interaction with an object using only the thumb and index finger (dashed), whereas the remaining digits "float" (solid). The configurations shown are of the entire hand.

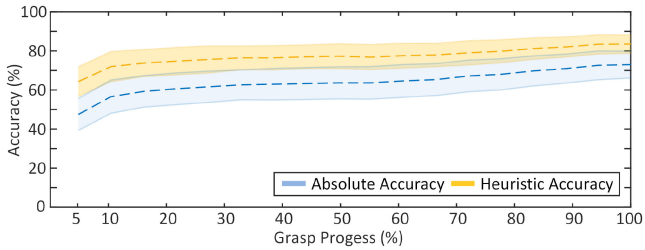

Fig. 6. This figure shows the prediction accuracy for all of the subjects using the trajectory-based prediction as a function of the grasp progress. The heuristic accuracy (orange) is based on the defined metrics while the absolute accuracy (blue) is based solely on metric (a). The dashed lines and shaded regions are the mean and standard deviation, respectively.

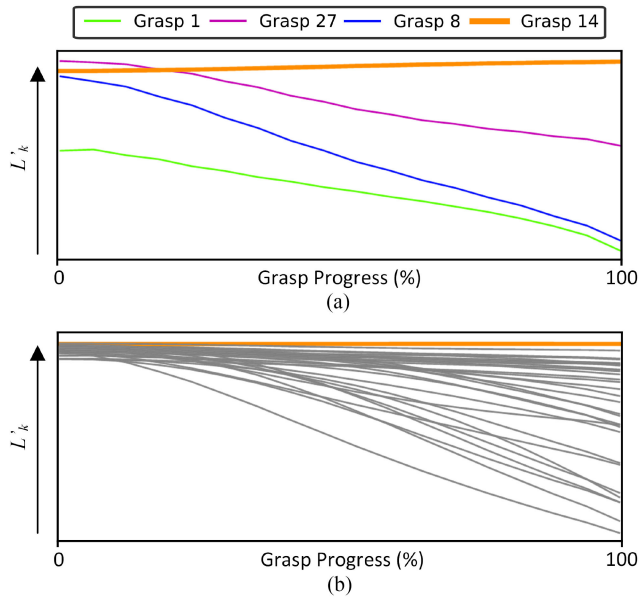

Fig. 7. Values for L'_k over the progress of the grasp while testing Grasp 14 tripod. The magnified view of the four most likely grasps (a) and the likelihood of all the grasps (b) are shown. Grasp 27 quadpod begins as the most likely grasp but is overtaken as more of the motion completes.

used a pneumatic actuation system, which was later replaced by series elastic actuator (SEA) modules allowing for precise force control capabilities on each individual finger applied as indicated in Fig. 8. The layout shown is replicated for each digit

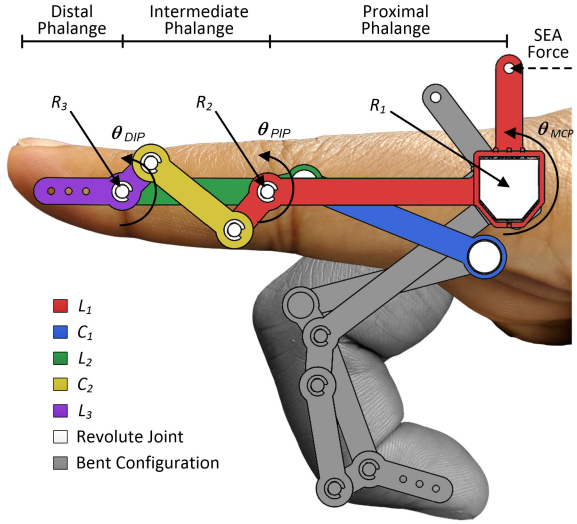

Fig. 8. Mechanical linkage layout for the RML Glove. Colored linkages L_i are associated with each phalange and C_i are complementary. The bent configuration of the finger when articulated is shown in gray.

and a modified version, with only a single four bar assembly, is used for the thumb.

For purposes of this experiment, the SEA is disconnected from the linkage mechanism so that the wearer of the glove can freely move and the only restrain on their motion is the kinematic coupling described typically by

$$\theta_{\text{MCP}} = 1.02\theta_{\text{PIP}} = 1.15\theta_{\text{DIP}}. \tag{21}$$

The angles used in this equation represent the joint angles of the glove that would ideally align with the corresponding joints on the finger. As discussed later in the results, this misalignment visible in Fig. 9 does not impact the effectiveness of the data collected.

The layout shown in Fig. 8 also locates a rotary potentiometer (the white hexagon at R_1) approximately at the MCP joint. The RML Glove does not allow for measurements of the finger abduction/adduction, instead only the five MCP joints are measured. The potentiometer, Bourns 3382, allows for measurement of the joint angles and thereby monitoring of the hand pose. The data from the potentiometer are read by a Teensy 3.6 microcontroller and recorded at 20 Hz for offline processing and evaluation of both prediction algorithms. Empirical evaluation of the sensor performance indicated presence of noise in the

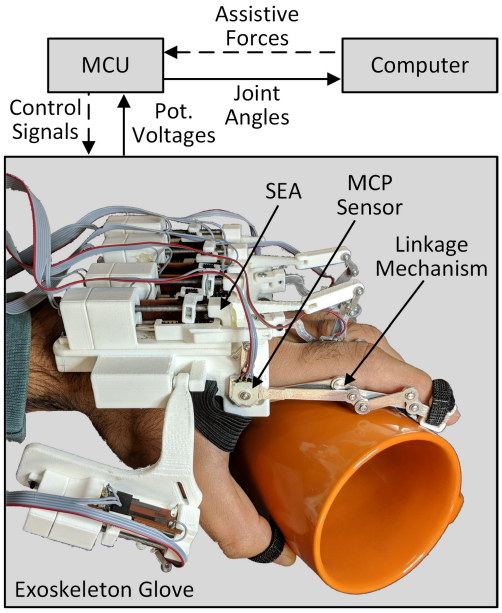

Fig. 9. Experimental setup and data flow of the measurements (solid arrows) and the control inputs (dashed arrows). The measurement data from the glove are sent to the MCU, which processes it into joint angles which it sends to the computer for use in the grasp prediction. The resulting assistive actions would then be passed back to the MCU which would control the actuators on the glove.

angle measurements of $\mathcal{U}(-6.3^\circ, 6.3^\circ)$. A diagram of the data flow for the experimental setup is shown in Fig. 9.

The kinematic coupling of the glove limits the ability of the wearer to perform many of the specialized grasps and explicitly any of those that violate its inherent kinematic coupling, such as the entire flat parallel group. However, it is designed to assist in the grasping of basic objects. To that end, the following geometrically dissimilar grasps were tested: medium cylinder, ring, tripod, quadpod, and ventral. Three objects were tested for each grasp, ten times each by the same user. Five of those ten trials were used to formulate the Gaussian processes shown in Fig. 10. The remaining five were used for the testing of the prediction. The data used in these experiments were based on the measured MCP joint angles. However, it can be seen in Fig. 9 that the joints of glove do not perfectly align with the joints of the finger. Despite this, the measured angles were still sufficiently unique to each grasp identification by the prediction algorithm. The misalignment between the mechanism and the hand does not violate this sufficiency, as the mechanism still bends with the finger, even if the relationship is not directly proportional as is the case when the glove is not an exact fit. In other words, it is assumed that there exists a bijective mapping between the mechanism angles and finger angles that are used for the prediction. The mapping itself would be different in different cases depending on the fit of the glove with the user's hand. Fit or user specific characteristics are automatically accounted for when training data are collected for each specific glove-user pair. Experimental data were collected from four healthy subjects with hand sizes appropriately matched to the size of the glove.

2) Experimental Results: The Gaussian process representation of the trajectories in the latent space for one of the subjects

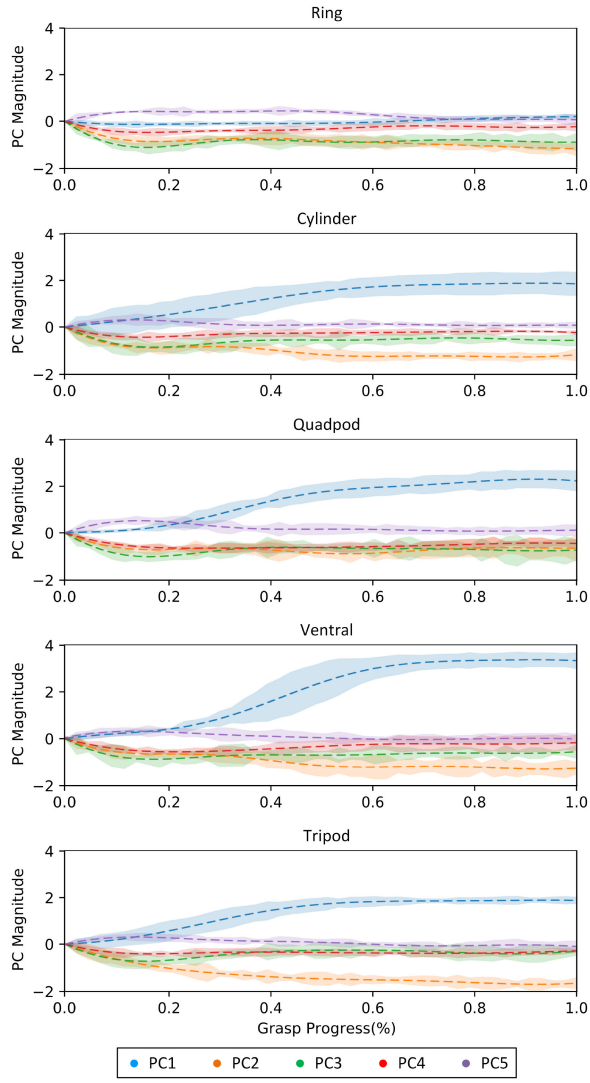

Fig. 10. Gaussian processes generated from the motion of a single subject completing the specified grasps while wearing the exoskeleton glove.

for each of the five grasps are shown in Fig. 10, where it can be seen that only five PCs are shown. Due to the five DOFs in the glove, after expansion of the motion according to (21), the weights for each of the PCs beyond the fifth were essentially zero, as expected. The trajectories shown are also repeatable and unique, despite the misalignment between the mechanism and the hand.

The average prediction accuracy, using the above-described trajectory-based prediction, at 25% of the motion, was 68.45% with a standard deviation of 6.21%. While not definitive, the kinematic coupling limits the amount of minute distinct motions, manifesting in the higher order PCs, that the user can make to conform to the grasped object. This can be seen in Fig. 10, where the PCs beyond the second take very similar paths. The prediction, after 75.00% and 100.00% of the motion completes, was 87.86% and 90.00% accurate. The confusion matrix of the hardware experiment prediction, at 25% of the completed motion, can be seen in Fig. 11, where both the means and standard deviations of each result are shown. While most of the grasps are predicted correctly, the ventral grasp results in

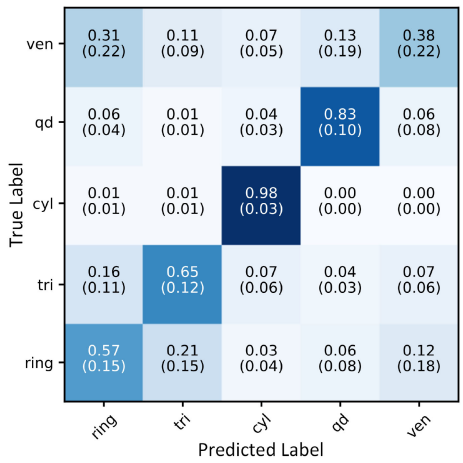

Fig. 11. Confusion matrix resulting from the trajectory-based prediction on the experimental glove data. The mean accuracy and (standard deviation) are shown.

a predicted ring grasp. It is unclear why this occurs since the geometric configurations are dissimilar; however, as more of the motion completes, the ventral grasps are correctly predicted as such. This trend aligns with what was seen in the simulation: more motion leads to more accurate predictions. Alternatively, the ring grasp is sometimes identified as the tripod grasp, which is somewhat understandable due to the extension of the middle finger in both grasps at the start of motion.

In regards to the dimensional reduction, for all of the grasps except the ring grasp, the first PC takes a similar path. It always appears to take an *S*-shaped path but ends at a different magnitude. This is due to that PC corresponding to small motion in the thumb and index finger, some motion in the middle finger, and large motion in the ring and pinky fingers. It therefore makes sense that the motion for the ring grasp has a low magnitude for this PC as the middle, ring, and pinky finger should stay almost entirely extended. Since it is still the combined similarity of all PCs being considered, the variability is significant enough for the prediction to be accurate.

IV. Future Work

The work presented here paves the way and yields necessary insights for future work in exoskeleton gloves. As mentioned previously, the grasp prediction algorithms discussed above could be used in the design of user guided control of exoskeleton gloves. The joints angles sensed by the glove, as well as the force exerted on the SEA by the user can be used to determine the specific grasp that the user was trying to achieve, based on which the necessary assistive force can be determined by the glove using a shifting haptic authority controller [27]. The assistive control action that the glove exerts control on the user u_{eu} is calculated as follows:

$$u_{eu} = \omega(\vec{\phi})\vec{u_p} + (1 - \omega(\vec{\phi}))\vec{u_u} \tag{22}$$

where $\vec{u_p}$ and $\vec{u_u}$ are the control actions, along each finger, or DOF in a more general case, to move the user toward the predicted configuration and the forces to amplify the user's current movements, respectively. The parameter $\omega(\vec{\phi})$ is a measure of the confidence in the prediction. The user control $\vec{u_u}$ will be an amplification of the motion of the user as measured by spring deflection in the SEA. Prior work by [28], which presents a positive feedback controller coupled with a low pass filter to maintain stability, will be implemented to determine $\vec{u_u}$. This controller will be tested on the exoskeleton system shown in Fig. 8.

After moving the hand to the desired grasping configuration, the next step is to determine how to exert the necessary forces to maintain a firm grasp on the object. Work presented in [29] used the iSAFER glove, an expansion of the SAFER glove presented in [30]. By using force-resistive sensors at the fingertips, the glove can detect when the object being held by the glove starts-to-slip, which when combined with the above controller, would allow for a start-to-finish control algorithm to assist the user in each phase of attempting to grasp an object.

The presented control scheme and prediction algorithm will be tested in real time on the RML Glove to evaluate the efficacy and qualitative usability of the assistive controller. The full system will be integrated into a mobile, lightweight unit that the user can wear throughout their day.

V. Conclusion

This paper presented two grasp prediction algorithms with the intention of using the grasp prediction to inform an assistive controller for an exoskeleton glove. Both algorithms begin by reducing the dimensionality of the data used in the prediction from 16 DOF (original hand data) to 6 DOF (principal components). Previous work demonstrates the beneficial effects of performing the prediction in this reduced dimensional space. The first algorithm performs a linear regression along the trajectory of each PC. The amount of data used to calculate the slope of the regression line decreases as the slope of the regression line increases. This mitigates the effects of the trajectory taking an unknown shape. The regression lines for each dimension are evaluated at a point forward in time that minimizes the error in configuration between each of the potential grasps that the user could be attempting. The second algorithm formulates the motion of each grasp as a Gaussian process that allows for the probabilistic comparison with the user's motion. The motion of the user is time scaled to maximize the log-likelihood of each possible grasp.

Both of the above grasp prediction algorithms were tested on HUST dataset that contains motion data from healthy users performing each of the grasps in the Feix taxonomy. An average accuracy of approximately 75% was achieved based on only approximately 25% of the grasping motion completed. While both predictions found grasps that were either geometrically or functionally similar, the trajectory-based algorithm was able to predict the exact grasp more consistently. Furthermore, the accuracy of the trajectory-based algorithm increased significantly as more of the grasp was completed and did not require a finite convergence time before rendering a prediction, unlike the first algorithm. In this way, the second algorithm is a more likely candidate for implementation as it can immediately be used to assist the wearer. Beyond simulated experiments, the trajectory-based prediction was tested on the RML Glove, which makes use of kinematic coupling in the finger joints to simplify the actuation and control of the glove. The glove was tested on

five grasps with results from four healthy subjects that were in line with the accuracies found during simulation.

We believe that the presented algorithms will increase the degree to which exoskeleton gloves can be integrated into ADL. They provide a way for users to overcome their physical impairments by augmenting their movements while relying on the user's capacity to make intelligent grasping choices.

REFERENCES

[1] M. Brault, "Americans with disabilities," U.S. Department of Commerce, Tech. Rep. P70-131, Jul. 2012. [Online]. Available: https://www.census.gov/library/publications/2012/demo/p70-131.html

[2] National Institute of Health, "Post-stroke rehabilitation," U.S. Department of Health and Human Services, Tech. Rep. 14 1846, 2014. [Online]. Available: https://www.stroke.nih.gov/documents/Post-Stroke_Rehabilitation_english_brochure_508C.pdf

[3] S. Arzillo, K. Gishen, and M. Askari, "Brachial plexus injury," *J. Craniofacial Surg.*, vol. 25, no. 4, pp. 1200–1206, Jul. 2014.

[4] National Center for Health Statistics, "Difficulties in physical functioning among adults aged 18 and over, by selected characteristics: United States, 2014," Centers for Disease Control and Prevention, 2014. [Online]. Available: https://ftp.cdc.gov/pub/Health_Statistics/NCHS/NHIS/SHS/2014_SHS_Table_A-10.pdf

[5] N. S. Ho *et al.*, "An EMG-driven exoskeleton hand robotic training device on chronic stroke subjects: Task training system for stroke rehabilitation," in *Proc. IEEE Int. Conf. Rehabil. Robot.*, Zurich, Switzerland, 2011, pp. 1–5. [Online]. Available: http://ieeexplore.ieee.org/document/5975340/

[6] Y. Yun *et al.*, "Maestro: An EMG-driven assistive hand exoskeleton for spinal cord injury patients," in *Proc. IEEE Int. Conf. Robot. Autom.*, Singapore, 2017, pp. 2904–2910.

[7] S.-S. Yun, B. B. Kang, and K.-J. Cho, "Exo-glove PM: An easily customizable modularized pneumatic assistive glove," *IEEE Robot. Autom. Lett.*, vol. 2, no. 3, pp. 1725–1732, Jul. 2017.

[8] C. J. Nycz, M. A. Delph, and G. S. Fischer, "Modeling and design of a tendon actuated soft robotic exoskeleton for hemiparetic upper limb rehabilitation," in *Proc. 37th Annu. Int. Conf. IEEE Eng. Med. Biol. Soc.*, Milan, Italy, 2015, pp. 3889–3892.

[9] E. Refour, B. Sebastian, and P. Ben-Tzvi, "Two-digit robotic exoskeleton glove mechanism: Design and integration," *J. Mech. Robot.*, vol. 10, no. 2, 2018, Art. no. JMR-17-1307.

[10] P. Heo, G. M. Gu, S.-J. Lee, K. Rhee, and J. Kim, "Current hand exoskeleton technologies for rehabilitation and assistive engineering," *Int. J. Precis. Eng. Manuf.*, vol. 13, no. 5, pp. 807–824, May 2012. [Online]. Available: http://link.springer.com/10.1007/s12541-012-0107-2

[11] A. DiDomenico and M. A. Nussbaum, "Estimation of forces exerted by the fingers using standardised surface electromyography from the forearm," *Ergonomics*, vol. 51, no. 6, pp. 858–871, 2008.

[12] J. T. Belter and A. M. Dollar, "Novel differential mechanism enabling two DOF from a single actuator: Application to a prosthetic hand," in *Proc. IEEE 13th Int. Conf. Rehabil. Robot.*, Seattle, WA, USA, June 2013, pp. 1–6.

[13] A. Úbeda, B. S. Zapata-Impata, S. T. Puente, P. Gil, F. Candelas, and F. Torres, "A vision-driven collaborative robotic grasping system teleoperated by surface electromyography," *Sensors*, vol. 18, no. 7, 2018, Art. no. 2366. [Online]. Available: https://www.mdpi.com/1424-8220/18/7/2366

[14] B. Noronha, S. Dziemian, G. A. Zito, C. Konnaris, and A. A. Faisal, ""Wink to grasp"—Comparing eye, voice & EMG gesture control of grasp with soft-robotic gloves," in *Proc. IEEE Int. Conf. Rehabil. Robot.*, London, U.K., 2017, pp. 1043–1048.

[15] J. Lin, Y. Wu, and T. Huang, "Modeling the constraints of human hand motion," in *Proc. Workshop Human Motion*, 2000, pp. 121–126. [Online]. Available: http://ieeexplore.ieee.org/document/897381/

[16] M. Gabiccini, G. Stillfried, H. Marino, and M. Bianchi, "A data-driven kinematic model of the human hand with soft-tissue artifact compensation mechanism for grasp synergy analysis," in *Proc. IEEE/RSJ Int. Conf. Intell. Robots Syst.*, Nov. 2013, pp. 3738–3745. [Online]. Available: http://ieeexplore.ieee.org/document/6696890/

[17] M. R. Cutkosky, "On grasp choice, grasp models, and the design of hands for manufacturing tasks," *IEEE Trans. Robot. Autom.*, vol. 5, no. 3, pp. 269–279, Jun. 1989.

[18] E. J. Weiss, "Muscular and postural synergies of the human hand," *J. Neurophysiology*, vol. 92, no. 1, pp. 523–535, 2004. [Online]. Available: http://jn.physiology.org/cgi/doi/10.1152/jn.01265.2003

[19] T. Feix, J. Romero, H. B. Schmiedmayer, A. M. Dollar, and D. Kragic, "The GRASP taxonomy of human grasp types," *IEEE Trans. Human-Mach. Syst.*, vol. 46, no. 1, pp. 66–77, Feb. 2016.

[20] M.-J. Liu, C.-H. Xiong, L. Xiong, and X.-L. Huang, "HUST dataset," 2016. [Online]. Available: http://www.handcorpus.org/?p=1596

[21] M. Santello, M. Flanders, and J. F. Soechting, "Postural hand synergies for tool use," *J. Neurosci.*, vol. 18, no. 23, pp. 10105–10115, 1998.

[22] J. Romero, T. Feix, H. Kjellstrom, and D. Kragic, "Spatio-temporal modelling of grasping actions," in *Proc. IEEE/RSJ Int. Conf. Intell. Robots Syst.*, Taipei, Taiwan, 2010, pp. 2103–2108.

[23] L. Zhang, W. Dong, D. Zhang, and G. Shi, "Two-stage image denoising by principal component analysis with local pixel grouping," *Pattern Recognit.*, vol. 43, no. 4, pp. 1531–1549, Apr. 2010. [Online]. Available: https://www.sciencedirect.com/science/article/pii/S0031320309003677

[24] R. J. Chauhan and P. Ben-Tzvi, "Latent variable grasp prediction for exoskeletal glove control," in *Proc. ASME Dyn. Syst. Control Conf.*, Atlanta, GA, USA, 2018, pp. 1–7.

[25] M. Liu and C. Xiong, "Synergistic characteristic of human hand during grasping tasks in daily life," in *Proc. 7th Int. Conf. Intell. Robot. App.*, Guangzhou, China, 2014, pp. 67–76.

[26] M. Ebden, "Gaussian processes: A quick introduction," Aug. 2015. [Online]. Available: https://arxiv.org/pdf/1505.02965.pdf

[27] D. A. Abbink, M. Mulder, and E. R. Boer, "Haptic shared control: Smoothly shifting control authority?" *Cognition, Technol., Work*, vol. 14, no. 1, pp. 19–28, 2012.

[28] U. Nagarajan, G. Aguirre-Ollinger, and A. Goswami, "Integral admittance shaping: A unified framework for active exoskeleton control," *Robot. Auton. Syst.*, vol. 75, pp. 310–324, Jan. 2016. [Online]. Available: https://www.sciencedirect.com/science/article/pii/S0921889015002031

[29] B. J. Lee, A. Williams, and P. Ben-Tzvi, "Intelligent object grasping with sensor fusion for rehabilitation and assistive applications," *IEEE Trans. Neural Syst. Rehabil. Eng.*, vol. 26, no. 8, pp. 1556–1565, Aug. 2018. [Online]. Available: https://ieeexplore.ieee.org/document/8387803/

[30] Z. Ma, P. Ben-Tzvi, and J. Danoff, "Sensing and force-feedback exoskeleton robotic (SAFER) glove mechanism for hand rehabilitation," in *Proc. ASME Int. Des. Eng. Tech. Conf. Comput. Inf. Eng. Conf.*, 2015, pp. 1–8.